MATERIALS PHYSICS AND MECHANICS RESEARCH ARTICLE

Submitted: October 29, 2025 **Revised: November 14, 2025** **Accepted: December 1, 2025**

Emission of lattice dislocations from triple junctions of grain boundaries with liquid-like inclusions near pores in high-temperature ceramics

M.Yu. Gutkin, N.V. Skiba ✉

Institute for Problems of Mechanical Engineering RAS, St. Petersburg, Russia

✉ nikolay.skiba@gmail.com

ABSTRACT

Theoretical model is suggested which describes the micromechanism of lattice dislocations emission from triple junctions of amorphous intercrystalline layers with pores and liquid-like inclusions in high-temperature ceramics. Within the model, the plastic deformation in ceramics under elevated temperatures is realized through the emission of lattice dislocations from triple junctions of grain boundaries and the subsequent glide of the emitted dislocations in the grain interior. In the exemplary case of high-temperature α-Al_2O_3 ceramics, a comparative analysis of the critical stresses for the emission of the lattice dislocations, and for their glide along the prismatic and basal slip planes in the grain interior depending on the deformation temperature was carried out in a wide temperature range from 300 to 1500 K. It is shown that the critical stress for the emission of the lattice dislocations decreases with both an increase in the length of the liquid-like inclusion and the deformation temperature, and increases with increasing the pore size.

KEYWORDS

high-temperature ceramics • pores • lattice dislocations • amorphous intercrystalline layers • deformation temperature liquid-liked inclusions

Funding. *This work has been supported by the grant of the Russian Science Foundation, RSF 23-19-00236.*

Citation: Gutkin MYu, Skiba NV. Emission of lattice dislocations from triple junctions of grain boundaries with liquid-like inclusions near pores in high-temperature ceramics. *Materials Physics and Mechanics*. 2026;54(1): 34–41. http://dx.doi.org/10.18149/MPM.5412026_5

Introduction

High-temperature ceramics (e.g., Al_2O_3, SiC, Si_3N_4, ZrO_2) often contain amorphous intercrystalline layers (AILs) and pores that influence their mechanical properties [1–10]. The liquid-like inclusions (LLIs) are nanoscale regions where the material locally behaves in a viscous or fluid-like manner due to the stress and the temperature conditions, facilitating the plastic flow in an otherwise brittle ceramic matrix [11–13]. The pores act as stress concentrators and nucleation sites for these inclusions [14,15].

The LLIs are usually small in size (of the order of tens of nanometers) that very complicates their experimental observations [6–9]. Thus, computer modeling [16–18] and analytical models [19–23] play a significant role in this field. The results of computer modeling [17,18] have stimulated the development of theoretical works [19–23] on the study of the generation and evolution of the LLIs in ceramic materials with AILs. Within these models, the plastic deformation occurs due to the generation and the propagation of the LLIs along the grain boundaries containing pores [23] and AILs [19]. In the case when the further development of LLIs along AILs is suppressed by their triple junctions, the LLIs

Publisher: Peter the Great St. Petersburg Polytechnic University

can act as effective stress concentrators inducing the implementation of other mechanisms of stress relaxation such as the nucleation of nanocracks on the LLIs [20], the LLIs overcoming the AIL triple junctions and penetrating into a neighboring AIL [21], and the subsequent emission of lattice dislocations from the AIL triple junctions with the LLIs [22].

Recent studies have revealed the formation of LLIs near pores in the high-temperature ceramics with AILs, which significantly affect the strength, the ductility, the creep resistance, the fracture toughness, etc. [4–6] of these ceramics. So, the development of the theoretical models describing the deformation mechanisms capable to improve the mechanical properties of the high-temperature ceramic materials with pores can significantly affect the range of their practical applications.

The main aim of this work is to develop a theoretical model of a micromechanism for the enhancement of plastic deformation through the emission of lattice dislocations (LDs) from the AIL triple junctions containing LLIs near pores in high-temperature ceramics at elevated temperatures.

Model

Consider a cylindrical pore of radius R_0 placed in an equilibrium triple junction of AILs containing an LLI of length L in a ceramic sample (Fig. 1). It is assumed that the LLI occupies the entire grain boundary reaching the opposite triple junction of AILs where its further propagation is suppressed. Within the model, this LLI as a source of mechanical stresses is modeled by a dipole of edge superdislocations with the Burgers vectors $\pm\mathbf{B}$ ($\pm B$-superdislocation dipole) and the arm $R_0 + L$ (Fig. 1).

Let us consider the process of the generation of a lattice dislocation (LD) with the Burgers vector $\mathbf{b}$ (b-LD) from the AIL triple junction under the external shear stress τ (Fig. 1) with taking into account the effect of the pore on the variation in the shear stress τ. In this case, the dipole of the $\pm B$-superdislocations acts as a stress concentrator facilitating the nucleation of the LD. This process becomes energetically favorable at $\tau \geq \tau_{c1}$, where τ_{c1} is some critical value of the external shear stress τ . However, the Peierls barrier

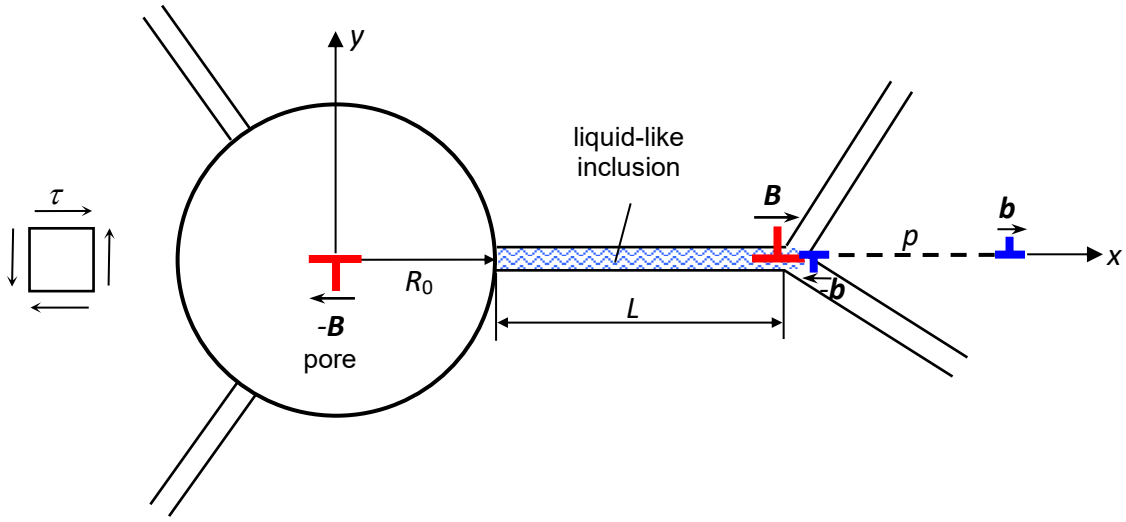

Fig. 1. Model of the LD emission from the AIL triple junction in the vicinity of a pore of radius R_0 and an LLI of length L under the external shear stress τ

hinders the movement of the emitted LD within the grain interior. Thus, the LD slip along one of the slip planes becomes possible at $\tau \geq \tau_{c2}$, where the τ_{c2} is a critical stress at which the LD can overcome the Peierls barrier.

According to the theory of defects in solids, the emission of the *b*-LD by the distance *p* from the AIL triple junction can be described as the appearance of an LD dipole with the Burgers vectors ±**b** (±*b*-LD dipole) and the arm *p* (Fig. 1). Previously, Glezer and Pozdnyakov [24] have developed a similar model although with no pore at the triple junction of grain boundaries. Thus, the LD emission can serve as an alternative mechanism of the plastic deformation enhancement in the high-temperature ceramics with LLIs in the vicinity of the pores.

Results

Consider the energy characteristics of the LD emission. The LD emission process is specified by the energy difference $\Delta W = W_2 - W_1$, where W_1 and W_2 are the total energies of the defect system before and after the LD emission (Fig. 1). The condition $\Delta W < 0$ determines the possibility of the generation of the ±*b*-LD dipole at the AIL triple junction. The energy difference ΔW is determined by the expression:

$$\Delta W = E_{self} + E_c + E\tau_{int}, \quad (1)$$

where E_{self} is the self-strain energy of the ±*b*-LD; $E_c \approx Gb2/[4\pi(1-\nu)]$ is the core energy of the emitted LD; *G* and *ν* are the shear modulus and the Poisson ratio, respectively; E_{int} is the energy of the elastic interaction between the ±*b*-LD dipole with the ±*B*-superdislocations, and E_τ is the effective work of the external shear stress τ spent to transfer the emitted LD over the distance *p*.

In accordance to the general approach [25], the self-strain energy E_{self} can be determined via the shear stress components of the ±*b*-LD dipole as follows:

$$E_{self} = \frac{b}{2}\int_{R_0+L+r_c}^{R_0+L+p-r_c}(\sigma_{xy}^{-b} + \sigma_{xy}^{b})dx, \quad (2)$$

where σ_{xy}^{-b} and σ_{xy}^{b} are the shear stresses of the $-b$-LD and *b*-LD located at a distance $d_1 = R_0 + L$ and $d_2 = R_0 + L + p$ from the pore center, respectively (Fig. 1).

With help of the Airy stress functions, Eq. (2) can be rewritten as follows:

$$E_{self} = \frac{b}{2}\left[\frac{\partial\Phi_1}{\partial y} + \frac{\partial\Phi_2}{\partial y}\right]_{x=R_0+L+r_c,y=0}^{x=R_0+L+p-r_c,y=0}, \quad (3)$$

where Φ_1 and Φ_2 are the Airy stress functions for the $-b$-LD and *b*-LD, respectively, that are given by the following well-known formulas [26]:

$$\Phi_1 = -\frac{bG}{2\pi(1-\nu)}y\left(\frac{1}{2}\frac{R_0^2}{r^2}\left(1-\frac{r^2r_1^2}{d_1^2r_2^2}\right)+ln\frac{rr_1}{r_2}\right),\ \Phi_2 = \frac{bG}{2\pi(1-\nu)}y\left(\frac{1}{2}\frac{R_0^2}{r^2}\left(1-\frac{r^2r_1^2}{d_2^2r_2^2}\right)+ln\frac{rr_1}{r_2}\right), \quad (4)$$

where $r = (x^2+y^2)^{1/2}$, $r_1 = (r^2+d_1^2+2rd_1)^{1/2}$, $r_2 = (r^2+d_2^2+2rd_2)^{1/2}$, $r_c \approx b$.

The energy E_{int} is given by a formula similar to Eq. (2):

$$E\int_{R_0+L}^{R_0+L+p}(\sigma_{xy}^{-B}{}^{B}_{xy})_{int}, \quad (5)$$

where σ_{xy}^{-B} and σ_{xy}^{B} are the shear stresses of the $-B$-superdislocation and *B*-superdislocation located in the center of a cylindrical pore and at a distance $d = R_0 + L$ from the pore center, respectively.

By analogy with the calculation of self-energy E_{self}, the interaction energy E_{in} is written using the Airy functions as:

$$E_{int}\left[\frac{\partial \Phi_3}{\partial y}+\frac{\partial \Phi_4}{\partial y}\right]_{x=R_0+L,y=0}^{x=R_0+L+p,y=0}, \quad (6)$$

where Φ_3 and Φ_4 are the Airy stress functions for the $-B$-superdislocation and B-superdislocation, respectively, that can be written as [26]:

$$\Phi_3=-\frac{BG}{2\pi(1-\nu)}y\left(\frac{1}{2}\frac{R_0^2}{r^2}+ln\,r\right),\ \Phi_4=\frac{BG}{2\pi(1-\nu)}y\left(\frac{1}{2}\frac{R_0^2}{r^2}\left(1-\frac{rr_3^2}{dr_4^2}\right)+ln\frac{rr_3}{r_4}\right), \quad (7)$$

where $r_3=(r^2+d^2+2rd)^{1/2}$ and $r_4=(r^2+d^2+2rd)^{1/2}$.

The energy E_τ that specifies the work of the external shear stress τ to move the b-LD over a distance p with taking into account the effect of the pore on the variation of the shear stress τ is given by equation [27]:

$$E_\tau=-bp\tau[1+2R_0^2/(R_0+L+p)^2-3R_0^4/(R_0+L+p)^4]. \quad (8)$$

With Eqs. (1)–(8), the energy difference ΔW can be calculated. Then the numerical calculation of the dependences $\Delta W(p)$ was carried out for different values of the external shear stress τ and the length L of the LLI in the exemplary case of high-temperature α-Al_2O_3 ceramics.

Since the material parameters (G and ν) exhibit weak dependence on the temperature, one can take G = 169 GPa and ν = 0.23 [28]. The magnitude of the LD Burgers vector b was chosen as $b \approx 0.27$ nm [29]. According to the model [24], the magnitude of the Burgers vectors of the $\pm B$-superdislocation dipole is equal to $\approx 0.025\,L$ at the low deformation temperature T = 300 K and $\approx 0.075\,L$ at the high deformation temperature T = 1500 K. The numerical calculations of the dependences

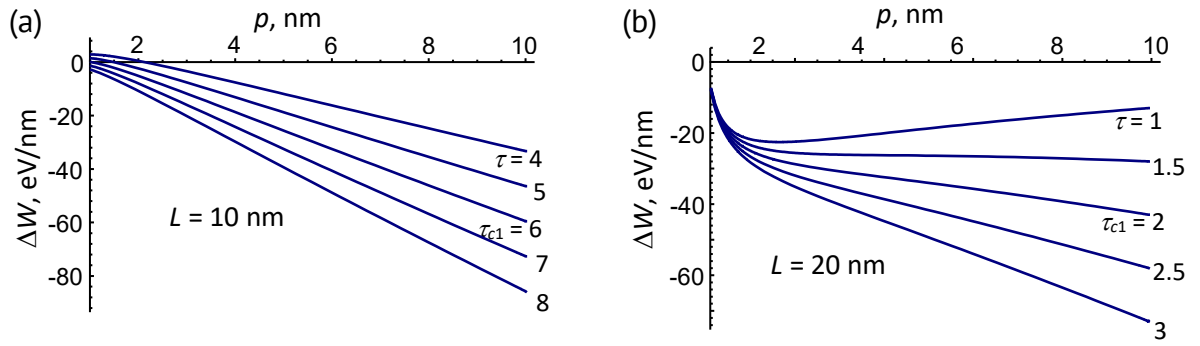

Fig. 2. The energy difference ΔW vs. the distance p at various values of the external shear stress τ, the pore radius R_0 = 10 nm, the distance L = 10 nm (a) and 20 nm (b), and the deformation temperature T = 300 K. The stress values are given in units of GPa

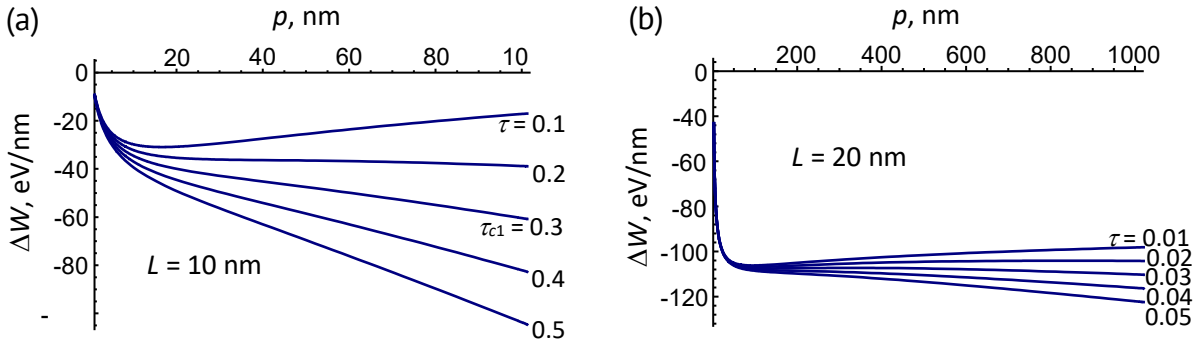

Fig. 3. The energy difference ΔW vs. the distance p at various values of the external shear stress τ, the pore radius R_0 = 10 nm, the distance L = 10 nm (a) and 20 nm (b), and the deformation temperature T = 1500 K. The stress values are given in units of GPa

$\Delta W(p)$ are illustrated in Figs. 2 and 3 for the pore radius R_0 = 10 nm, the two different values of L: L = 10 nm (Figs. 2(a) and 3(a)) and 20 nm (Figs. 2(b) and 3(b)), different values of the external shear stress τ, and the deformation temperatures T = 300 K (Fig. 2) and T = 1500 K (Fig. 3).

With the help of the conditions $\Delta W \leqslant 0$ at p = 1 nm and $\partial\Delta W/\partial p < 0$ for $p > 1$ nm, the critical value τ_{c1} of the external shear stress τ can be calculated. At $\tau \geq \tau_{c1}$, the LD emission is occurred in a barrier-less manner. As it can be seen from Figs. 2 and 3, the higher is the deformation temperature and the bigger is the distance L, the lower is the value of the critical stress τ_{c1} which determines the LD emission from the AIL triple junction in the vicinity of the pore. A similar calculation method can be used to determine the critical stress τ_{c1} for other deformation temperatures.

It should be noted that the implementation of the dislocation sliding along slip planes can be realized by applying an external shear stress that exceeds a certain critical value τ_{c2} at which the LD can overcome the Peierls barrier. The strong dependence of the Peierls barrier on temperature determines the temperature dependence of the critical stress τ_{c2} which (in the case of α-Al_2O_3 ceramics) is given by the following equations [30] for the LD slip along the basal (τ_{c2b}) and prismatic slip (τ_{c2p}) planes:

$$\tau_{c2b} = \tau_{0b} e^{-0.0052 \rightleftarrows T}, \quad (9)$$

$$\tau_{c2p} = \tau_{0p} e^{-0.0026T}, \quad (10)$$

where τ_{c0b} = 109 GPa and τ_{c0p} = 9 GPa.

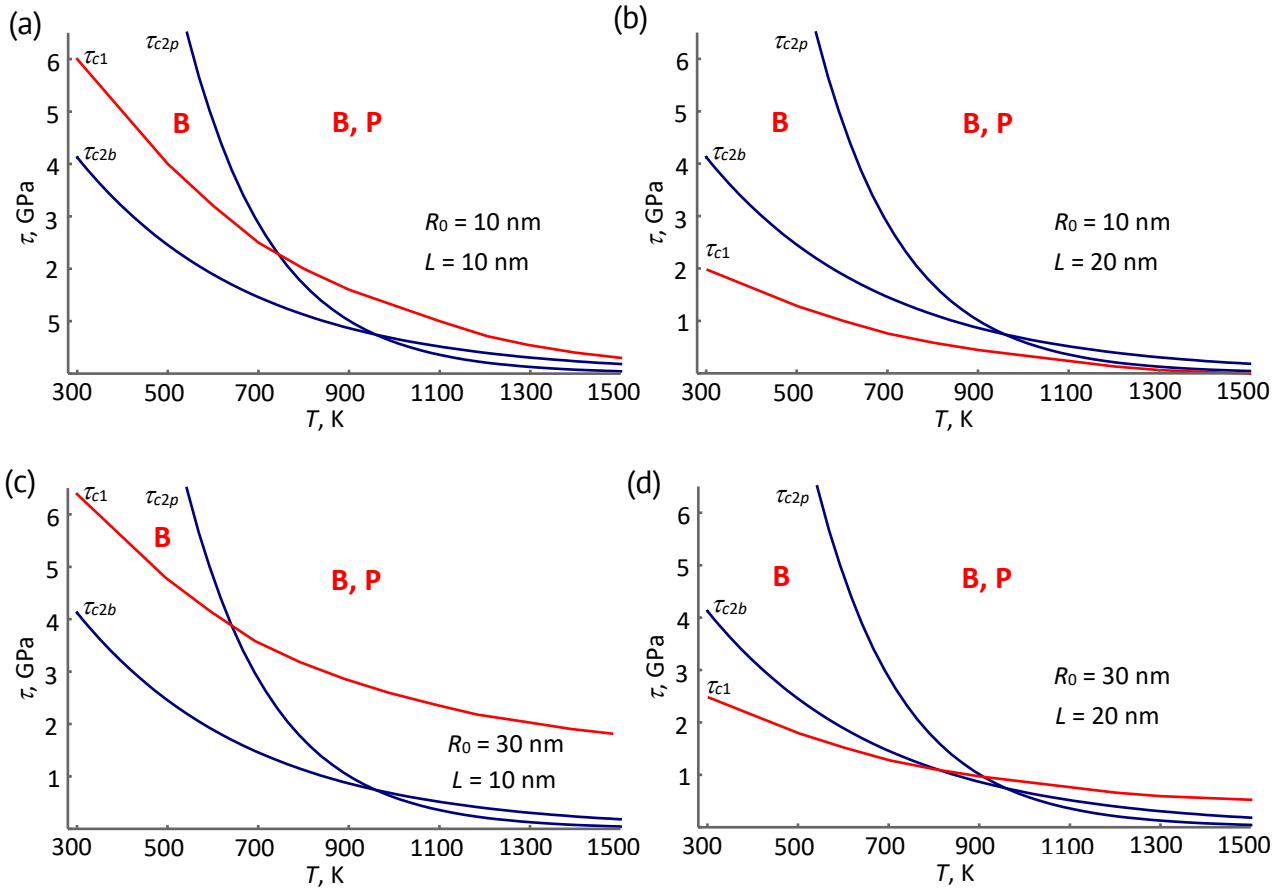

Fig. 4. The critical stresses τ_{c1} and τ_{c2} vs. the deformation temperature T at the LLI length, L = 10 nm (a,c) and (b,d) 20 nm, and the pore radius, R_0 = 10 nm (a,b) and 30 nm (c,d). Regions B and P determine the critical stresses and the deformation temperatures for the basal and prismatic slip planes, respectively

Using Eqs. (1)–(10), one can calculate the dependences $\tau_{c1}(T)$ and $\tau_{c2}(T)$ of the critical stresses τ_{c1} and τ_{c2} on the deformation temperature T in the case of the high-temperature α-Al_2O_3 ceramics with pores at the AIL triple junctions. The numerical calculation of the temperature dependences $\tau_{c1}(T)$ and $\tau_{c2}(T)$ are presented in Fig. 4 for the LLI length, L = 10 nm (Fig. 4(a,c)) and 20 nm (Fig. 4(b,d)), and the pore radius, R_0 = 10 nm (Fig. 4(a,b)) and R_0 = 30 nm (Fig. 4(c,d)). In the model, the LD emission from the AIL triple junction in the vicinity of the pore becomes energetically favorable if the condition $\tau \geq \tau_{c1}$ is satisfied. On the other side, the fulfilment of the conditions $\tau \geq \tau_{c2p}$ and/or $\tau \geq \tau_{c2b}$ determines the ability of the emitted LD to slide along one of the slip planes: the basal slip plane (region B in Fig. 4) or the prismatic slip plane (region P in Fig 4).

An increase in the LLI length L and a decrease in the pore radius R_0 contribute to the expansion of the ranges of the critical stresses and the deformation temperatures (regions B and P, Fig. 4) at which the sliding of the emitted LD in the grain interior is energetically favorable. Obviously, the effect of the LLI length L is explained by the corresponding increase in the stress of the $\pm B$-superdislocation dipole with its arm and the corresponding decrease in the image force attracting the emitted LD to the pore surface. The effect of the pore radius R_0 is also caused by the diminishing attracting image force on the LD.

Thus, the presence of pores makes it harder the emission of LDs from the neighboring AIL triple junctions. The bigger is the pore radius the higher is the critical stress for the dislocation emission.

Conclusions

A micromechanism has been suggested which describes the implementation of the plastic deformation in the high-temperature porous ceramics with liquid-like inclusions (LLIs) in amorphous intercrystalline layers (AILs). In the framework of the model, the evolution of the LLIs is suppressed by AIL triple junctions and they serve as effective stress concentrators which are capable to induce the action of alternative mechanisms of plasticity under elevated temperatures. Such an alternative mechanism of the plastic deformation enhancement can be the emission of lattice dislocation (LDs) from the triple junctions of the AILs containing the LLIs, and the subsequent glide of the emitted LDs in the grain interior along slip planes under the combined action of the external shear stress and the stress field of the LLIs. The presence of pores in AILs and their triple junctions has been expected to effect upon the emission critical conditions. Using α-Al_2O_3 nanoceramics as an example, the energy characteristics for the LD emission near a pore have been calculated. Also, a comparative analysis of the critical stresses for the emission of the LDs and for their slide along the prismatic and basal slip planes depending on the deformation temperature has been carried out in a wide temperature range from 300 to 1500 K.

It has been shown that, while the LLIs pressed to AIL triple junctions can effectively stimulate the emission of LDs from these triple junctions, the presence of pores in the neighboring AIL triple junctions makes it harder the emission of LDs. The bigger is the pore radius the higher is the critical stress for the LD emission.

It is worth mentioning that understanding the alternative mechanisms of the plastic deformation enhancement guides the engineering of the ceramic microstructures to

optimize the pore distribution and the amorphous layer properties, aiming at improved the mechanical properties (the fracture toughness and the ductility) at the elevated temperatures.

CRediT authorship contribution statement

Mikhail Yu. Gutkin: writing – review & editing; **Nikolay V. Skiba**: writing – original draft.

Conflict of interest

The authors declare that they have no conflict of interest.

References

1. Maniakin P, Shalagaev SG, Archakov IYu, Konakov YaV, Kurapova OYu, Konakov VG. In-situ high-temperature bending strength measurement of YSZ ceramics manufactured using novel B2O3-based glass binder. *Materials Physics and Mechanics.* 2024;52(2): 64–75.
2. Koch CC, Ovid'ko IA, Seal S, Veprek S. *Structural nanocrystalline materials: fundamentals and applications.* Cambridge: Cambridge University Press; 2007.
3. Liu J, Huo W, Zhang X, Ren B, Li Y, Zhang Z, Yang J. Optimal design on the high-temperature mechanical properties of porous alumina ceramics based on fractal dimension analysis. *Journal of Advanced Ceramics.* 2018;7: 89–98.
4. Zhang D, Yu R, Feng X, Guo X, Yang Y, Xu X. Enhanced mechanical properties of Al2O3 nanoceramics via low temperature spark plasma sintering of amorphous powders. *Materials.* 2023;16(16): 5652.
5. Wang L, An L, Zhao J, Shimai S, Mao XJ, Zhang J, Liu J, Wang SW. High-strength porous alumina ceramics prepared from stable wet foams. *Journal of Advanced Ceramics.* 2021;10: 852–859.
6. Zhang ZL, Sigle W, Koch CT, Rühle M. Dynamic behavior of nanometer-scale amorphous intergranular film in silicon nitride by in situ high-resolution transmission electron microscopy. *Journal of the European Ceramic Society.* 2011;31(9): 1835–1840.
7. Krasnitckii SA, Sheinerman AG, Gutkin MYu. Brittle vs ductile fracture behavior in ceramic materials at elevated temperature. *Materials Physics and Mechanics.* 2024;52(2): 82–89.
8. Subramaniam A, Koch CT, Cannon RM, Rühle M. Intergranular glassy films: An overview. *Materials Science and Engineering A.* 2006;422(1–2): 3–18.
9. Kleebe HJ. Structure and chemistry of interfaces in Si3N4 ceramics studied by transmission electron microscopy. *Journal of the Ceramic Society of Japan.* 1997;105(1222): 453–475.
10. Golubev SN, Kurapova OYu, Archakov IYu, Konakov VG. Characterization of a high temperature ceramics produced via two-step additive manufacturing. *Open Ceramics.* 2021;7: 100165.
11. Hulbert DM, Jiang D, Kuntz JD, Kodera Y, Mukherjee AK. A low-temperature high-strain-rate formable nanocrystalline superplastic ceramic. *Scripta Materialia.* 2007;56(12): 1103–1106.
12. Xu X, Nishimura T, Hirosaki N, Xie R-J, Yamamoto Y, Tanaka H. Superplastic deformation of nano-sized silicon nitride ceramics. *Acta Materialia.* 2006;54(1): 255–262.
13. Chen D, Zhang XF, Ritchie RO. Effects of grain-boundary structure on the strength, toughness, and cyclic-fatigue properties of a monolithic silicon carbide. *Journal of the American Ceramic Society.* 2000;83(8): 2079–2081.
14. Rice RW. Limitations of pore-stress concentrations on the mechanical properties of porous materials. *Journal of Materials Science.* 1997;32: 4731–4736.
15. Suleiman B, Zhang H, Ding Y, Li Y. Microstructure and mechanical properties of cold sintered porous alumina ceramics. *Ceramics International.* 2022;48(10): 13531–13540.
16. Mo YF, Szlufarska I. Simultaneous enhancement of toughness, ductility, and strength of nanocrystalline ceramics at high strain-rates. *Applied Physics Letters.* 2007;90(18): 181926.
17. Demkowicz MJ, Argon AS. High-density liquidlike component facilitates plastic flow in a model amorphous silicon system. *Physical Review Letters.* 2004;93(2):025505.

18. Demkowicz MJ, Argon AS. Liquidlike atomic environments act as plasticity carriers in amorphous silicon. *Physical Review B.* 2005;72(24): 245205.
19. Gutkin MYu, Ovid'ko IA. A composite model of the plastic flow of amorphous covalent materials. *Physics of the Solid State.* 2010;52(1): 58–64.
20. Gutkin MYu, Ovid'ko IA. Plastic flow and fracture of amorphous intercrystalline layers in ceramic nanocomposites. *Physics of the Solid State.* 2010;52(4): 718–727.
21. Gutkin MYu, Mikaelyan KN. A model of strain hardening in nanoceramics with amorphous intercrystalline layers. *Physics of Complex Systems.* 2021;2(2): 51–60.
22. Gutkin MYu, Skiba NV. Emission of lattice dislocations from triple junctions of grain boundaries in high-temperature ceramics with amorphous intercrystalline layers. *Materials Physics and Mechanics.* 2024;52(1): 39–48.
23. Gutkin MYu, Krasnitckii SA, Skiba NV. Formation of liquid-like inclusions near pores in amorphous intercrystalline layers in high-temperature ceramics. *Materials Physics and Mechanics.* 2024;52(6): 8–16.
24. Glezer A, Pozdnyakov V. Structural mechanism of plastic deformation of nanomaterials with amorphous intergranular layers. *Nanostructured Materials.* 1995;6(5–8): 767–769.
25. Mura T. *Micromechanics of defects in solids.* Dordrecht: Springer Dordrecht; 1987.
26. Eshelby JD. Boundary problems. In: Nabarro FRN. (eds.) *Dislocations in solids. Vol. 1.* Amsterdam: North-Holland Publishing Company; 1979. p. 167–221.
27. Asaro RJ, Lubarda VA. *Mechanics of Solids and Materials.* Cambridge: Cambridge University Press; 2006.
28. Smithells CJ. (Ed.) *Metals reference book. 5th ed.* London: Butterworths; 1976.
29. Lagerlöf KPD, Heuer AH, Castaing J, Rivière JP, Mitchell TE. Slip and twinning in sapphire (α-Al2O3). *Journal of the American Ceramic Society.* 1994;77(2): 385–397.
30. Choi SM, Awaji H. Nanocomposites – a new material design concept. *Science and Technology of Advanced Materials.* 2005;6: 2–10.